Wind and Structures, *Vol. 20, No. 2 (2015) 249-274*
DOI: http://dx.doi.org/10.12989/was.2015.20.2.249

Nonlinear dynamic performance of long-span cable-stayed bridge under traffic and wind

Wanshui Han[1], Lin Ma[2a], C.S. Cai[3b], Suren Chen[4c] and Jun Wu[*1d]

[1]Highway College, Chang'an University, Xi'an, Shaanxi, 710064, China
[2]Department of Civil and Environmental Engineering, Hohai University, Nanjing, Jiangsu 210098, China
[3]Department of Civil and Environmental Engineering, Louisiana State University, Baton Rouge, LA 70803. USA
[4]Department of Civil and Environmental Engineering, Colorado State University, Fort Collins, CO 80523, USA

(Received November 19, 2014, Revised January 5, 2015, Accepted January 8, 2015)

Abstract. Long-span cable-stayed bridges exhibit some features which are more critical than typical long span bridges such as geometric and aerodynamic nonlinearities, higher probability of the presence of multiple vehicles on the bridge, and more significant influence of wind loads acting on the ultra high pylon and super long cables. A three-dimensional nonlinear fully-coupled analytical model is developed in this study to improve the dynamic performance prediction of long cable-stayed bridges under combined traffic and wind loads. The modified spectral representation method is introduced to simulate the fluctuating wind field of all the components of the whole bridge simultaneously with high accuracy and efficiency. Then, the aerostatic and aerodynamic wind forces acting on the whole bridge including the bridge deck, pylon, cables and even piers are all derived. The cellular automation method is applied to simulate the stochastic traffic flow which can reflect the real traffic properties on the long span bridge such as lane changing, acceleration, or deceleration. The dynamic interaction between vehicles and the bridge depends on both the geometrical and mechanical relationships between the wheels of vehicles and the contact points on the bridge deck. Nonlinear properties such as geometric nonlinearity and aerodynamic nonlinearity are fully considered. The equations of motion of the coupled wind-traffic-bridge system are derived and solved with a nonlinear separate iteration method which can considerably improve the calculation efficiency. A long cable-stayed bridge, Sutong Bridge across the Yangze River in China, is selected as a numerical example to demonstrate the dynamic interaction of the coupled system. The influences of the whole bridge wind field as well as the geometric and aerodynamic nonlinearities on the responses of the wind-traffic-bridge system are discussed.

Keywords: bridges; long span; traffic; geometric nonlinearity, aerodynamic nonlinearity; wind field; nonlinear iteration method

1. Introduction

With the rapid development of the economy and the progress of engineering materials and

*Corresponding author, Professor, E-mail: jun.wu@chd.edu.cn
[a] Assistant Professor, E-mail: malinmalin8005@126.com
[b] Professor, E-mail: C.S.CAI@lsu.edu
[c] Associate Professor, E-mail: suren.chen@colostate.edu
[d] Associate Professor, E-mail: jun.wu@chd.edu.cn

http://www.techno-press.org/?journal=was&subpage=8 ISSN: 1226-6116 (Print), 1598-6225 (Online)

construction techniques, many long-span bridges have been built recently or are now under construction in China. For example, the Sutong Bridge in China is a long-span cable-stayed bridge with the main span of 1,088 m. Generally speaking, these long-span cable-stayed bridges have high flexibility and low structural damping, which makes them much more susceptible to the aerodynamic effects than their counterparts with shorter spans (Simiu and Scanlan 1996). Besides, these bridges are often close to coastal areas or crossing large rivers, experiencing complex wind environment frequently. Since it was opened to traffic in May 2008, the Sutong Bridge has already experienced several typical typhoon events including Typhoon Fung-Wong and Typhoon Kalmaegi (Wang *et al*. 2013). To accurately predict the performance of these bridges under different wind and traffic conditions is crucial to assessing the safety of the bridge, passing vehicles, driving comfort, and long-term bridge fatigue performance.

A series of studies on coupled wind-vehicle-long span bridge systems (Xu and Guo 2003, Cai and Chen 2004, Cheung and Chan 2010, Chen *et al*. 2011, Ma and Han 2014) have been carried out during the last decade. Compared to typical long-span bridges with much shorter spans, long-span bridges, like the Sutong Bridge, exhibit some unique characteristics, such as more slender bridge structures and considerably larger number of moving vehicles on the bridge at a time. As a result, the wind loads acting on these bridges become more complex and the wind loads acting on the bridge tower and cables may become non-trivial as compared to those on the bridge deck. For example, the main tower of the Sutong Bridge is about 300-m high and the length of the longest cable is about 577 m. Therefore, the wind forces acting on the pylons and cables may not only greatly contribute to the bridge responses directly but also may strengthen the dynamic interaction between the bridge and the vehicles. Because of the increase of the number of vehicles simultaneously moving on the bridge, the computational demand of wind-traffic-bridge interaction analysis will exponentially increase (Chen and Cai 2007). As a result, more efficient simulation algorithms become important in order to analyze long-span bridges with reasonable computational costs. In addition, the slenderness nature of these bridges may make the geometric and aerodynamic nonlinearities significant for these bridges.

In most existing studies, the mode superposition method was typically adopted to develop the wind-traffic-bridge interaction model (Cai and Chen 2004, Chen and Wu 2010, Chen *et al*. 2011). Basically a certain number of modes are selected based on modal analysis results of the bridge from some commercial finite element method (FEM) software, with higher modes being truncated. Although such an approach usually works well on typical long-span bridges, it may pose some challenges on long-span bridges for two reasons: (1) it is important to determine how many vibration modes of the bridge should be involved in the analysis so as to ensure the accuracy without excessive computational efforts for the stress and acceleration responses analysis (Li *et al*. 2010, Xu *et al*. 2010). It may become more difficult to choose appropriate modes for the coupled analysis when the bridge becomes more slender and more complex; and (2) the mode superposition approach is generally based on linear assumption and will not be applicable to structures with considerable nonlinear effects. Therefore, for these long-span bridges, some improved analytical approach and simulation tools still need to be developed to address these challenges.

In the following sections, a three-dimensional nonlinear analytical model based on a direct FEM formulation of bridge structures will be developed, which can be used to conduct the dynamic analysis of long cable-stayed bridges under the combined loads of the stochastic traffic and wind. In the proposed model, several major improvements over the existing studies are made. Firstly, the FEM formulation of the bridge structure can avoid the challenge of mode selection while various geometric and aerodynamic nonlinearities can be appropriately considered. These nonlinearities include cable sag, force-bending moment interaction in the bridge deck and towers, and changes of bridge geometry due to large displacements as well as aerodynamic nonlinearity such as the effective attack angle effect and the nonlinear components of self-excited forces, etc. Secondly, the equations of motion of the coupled wind-traffic-bridge system are derived and solved with a nonlinear iterative procedure which can considerably improve the calculation efficiency of long-span bridges. Lastly, the wind loads on the whole long-span bridge, including bridge deck, pylons, and cables, will be considered. The Sutong Bridge across the Yangtze River in China is selected as a numerical example to demonstrate the proposed methodology.

2. Modeling of wind-traffic-bridge system

2.1 Three-dimensional wind field simulation on the bridge

Wind velocity is not only the function of time, but also varies with the spatial position (x, y, z). Hence, the complete wind velocity field should be treated as a multidimensional, multivariate, homogeneous Gaussian stochastic process. In practice, the wind field simulation is usually further simplified as a combination of three independent, one-dimensional, multivariate stochastic processes, ignoring the coherence between different dimensions. Shinozuka and Deodatis (1991) developed the classical spectral representation method to simulate an ergodic stochastic wind velocity field. While Cao and Xiang (2000) greatly improved the efficiency by introducing an explicit Cholesky decomposition of the special power spectrum density (PSD) matrix, this method has two limitations, i.e., the spacing of the simulation points must be identical and the auto-power spectra at all the simulation points must be the same (i.e., the simulation points need to have the same elevation). In order to simulate the wind fields on all the major components of a long-span cable-stayed bridge, such as bridge deck, pylons, cables, and piers, a large number of wind velocity histories at many points need to be simulated simultaneously. As a result, the traditional algorithm (Sinozuka and Deodatis 1991) becomes computationally prohibitive and the explicit method (Cao and Xiang 2000) is not feasible.

To resolve these issues, a modified spectral representation method was proposed. In this method, the number of Cholesky decomposition of the cross power spectral density (PSD) matrix is reduced and the non-decomposition frequency points are approximated by the interpolation technique. Because of all these, the modified spectral representation method is more efficient and requires less computational resources, making it very suitable for simulating the spatial wind fields of long-span bridges. This approach is implemented in the present study to simulate the fluctuating wind field of the whole bridge and is briefly introduced next.

The samples of a one-dimensional multivariate Gaussian process with zero mean can be simulated by using the following equations

$$f_j(t) = 2\sqrt{\Delta\omega}\sum_{m=1}^{j}\sum_{l=1}^{N}\left|H_{jm}(\omega_{ml})\right|\cos(\omega_{ml}t - \theta_{jm}(\omega_{ml}) + \phi_{ml}) \tag{1}$$

$$\begin{cases} \Delta\omega = \omega_u / N \\ \theta_{jm}(\omega_{ml}) = \tan^{-1}\left\{\dfrac{\mathrm{Im}[H_{jm}(\omega_{ml})]}{\mathrm{Re}[H_{jm}(\omega_{ml})]}\right\} \\ \omega_{ml} = (l-1)\Delta\omega + m/n\Delta\omega \end{cases} \tag{2}$$

where j = 1,2,…,n. n is the number of the wind field simulation points on the bridge; N is the number of frequency intervals, often being a sufficiently large positive integer; $\Delta\omega$ is the frequency interval, and $\Delta\omega=\omega_u/N$; ϕ_{ml} is a set of independent random phase angles uniformly distributed between 0 and 2π with a density of $1/2\pi$; ω_{ml} is the double-indexing of the frequency, and $\omega_{ml} = (l-1)\Delta\omega + m/n\Delta\omega$; ω_u is the upper cutoff frequency; $\theta_{jm}(\omega_{ml})$ is the complex angle of $H_{jm}(\omega_{ml})$; and $f_j(t)$ is a sample of the stochastic wind speed history which will be used to determine the wind loads on both the vehicles and the whole bridge at each time step.

$H_{jm}(\omega_{ml})$, a typical element of the lower triangular matrix, is obtained in the following Cholesky's decomposition of the cross-spectral density matrix $S^0(\omega)$ of one dimensional multivariate Gaussian process

$$S^0(\omega) = H(\omega)H^{T*}(\omega) \tag{3}$$

where $H(\omega)$ is the lower triangular matrix; and $H^{T*}(\omega)$ is the complex-conjugate matrix of $H(\omega)$.

Since $H(\omega)$ is the function of ω, the Cholesky's decomposition of $S^0(\omega)$ should be performed at every ω_{ml} as shown in Eq. (1), which is a computational expensive process. In practice, the cross-spectral density of different spatial points is usually expressed in a real function and the cross PSD matrix $\mathbf{S}^0(\omega)$ is a real symmetric matrix. Therefore, the lower triangular matrix is also a real symmetric matrix. Because every element of $H(\omega)$ varies with the frequency continuously, an appropriate interpolation function can be chosen to reduce the decomposition number of $S^0(\omega)$ and improve the calculation efficiency. Due to its higher accuracy than the linear interpolation, a thrice Lagrange polynomial interpolation is used in the present study to acquire the approximate $\tilde{H}_{jm}(\omega_{ml})$ at the non-decomposition frequency points ω_{ml} as

$$\tilde{H}_{jm}(\omega_{ml}) = \sum_{l=i-1}^{i+2} H_{jm}(\omega_l)L_l(\omega_{ml}) \tag{4}$$

where $L_l(\omega_{ml})$ is the Lagrange interpolation function and $H_{jm}(\omega_l)$ is an element of the lower triangular matrix at the frequency decomposition point ω_l.

After applying the approximated interpolation of $H(\omega)$, the simulation of a random wind velocity can be derived from Eq. (1) as

$$f_j(t) = 2\sqrt{\Delta\omega}\sum_{m=1}^{j}\sum_{l=1}^{N} \tilde{H}_{jm}(\omega_{ml})\cos(\omega_{ml}t - \theta_{jm}(\omega_{ml}) + \phi_{ml}) \tag{5}$$

To improve the computational efficiency, the simulation process is carried out by using the Fast Fourier transform technique (Cao 2000).

2.2 Vehicle model and probabilistic traffic flow simulation with Cellular Automaton model

Each vehicle is modeled as a combination of several rigid bodies connected by several axle mass blocks, springs, and damping devices (Han *et al*. 2014a). The tires are considered as lower suspension systems connecting the axle sets to the bridge deck. The upper suspensions are used to connect the axle sets and the vehicle bodies, and the suspension systems are idealized as linear elastic spring elements and dashpots. In order to cover the typical vehicles traveling on highway bridges, a comprehensive vehicle model database is developed which can numerically simulate vehicles on highway roads or bridges with axle number varying from two to six (Han *et al*. 2014b).

There is a high probability of the simultaneous presence of multiple vehicles on a long-span bridge. The realistic traffic flow on these bridges exhibits complicated characteristics in terms of vehicle number, vehicle type combination, and drivers' operation such as lane changing, acceleration, or deceleration on long-span bridges. In order to apply more realistic traffic loading on long-span bridges, the traffic flow acting on the bridge is simulated through the cellular automation (CA) traffic model, which is a time-discrete and space-discrete stochastic simulation of spontaneous traffic flows by defining the basic traffic conditions (Chen and Wu 2011).

3. Dynamic interactions among wind, traffic and bridge

3.1 Wind-bridge interaction

Wind forces acting on a long cable-supported bridge are mainly the static wind forces caused by the mean wind, the buffeting forces caused by the turbulent wind, and the self-excited forces caused by the interaction between the wind and bridge motion. In most previous studies, only the wind loads acting on the bridge deck were usually simulated (Ding and Lee 2000, Xu and Guo 2003, Cai and Chen 2004, Cheung and Chan 2010) while the wind forces acting on other components of the bridge (cables, pylons, and piers) were usually neglected because of their relative insignificance. In order to achieve more realistic and reliable results for long-span cable-stayed bridges, the static wind forces and buffeting forces acting on the whole bridge, including the deck, cables, pylons, and piers are simultaneously considered. Furthermore, the static wind forces, the buffeting forces, and the self-excited forces are all functions of the effective attack angle between the wind flow and the deformed bridge deck. In the present study, the varied static and aerodynamic forces under different torsional angles caused by wind will be rationally considered.

3.2 Static wind loads acting on the whole bridge

The static wind forces on the whole bridge can be divided into two parts, (1) the aerostatic lift force, drag force, and torsional moment acting on the bridge deck; and (2) the drag force acting on the pylons, cables, and piers.

The aerostatic forces acting on the bridge deck change with the torsional deformation of the main girders and the torsional deformations of deck change along the bridge longitudinal axis. Therefore, the static wind force acting on the bridge deck is a function of the spatial deformation. The aerostatic force acting on per unit length of the bridge deck can be expressed as follows

$$L_{st} = \frac{1}{2}\rho U_z^2 C_L(\theta) B_d\,;\; D_{st} = \frac{1}{2}\rho U_z^2 C_D(\theta) B_d\,;\;\; M_{st} = \frac{1}{2}\rho U_z^2 C_M(\theta) B_d^2 \tag{6}$$

where ρ is the air density; U_z is the mean wind velocity at the elevation of the bridge deck z; B_d is the bridge deck width; θ is the wind attack angle; $C_L(\theta)$, $C_D(\theta)$, and $C_M(\theta)$ are the lift, drag, and moment static wind force coefficients for the bridges corresponding to the wind angle θ, respectively, which are usually obtained from wind tunnel tests of the bridge deck.

The static wind drag forces acting on pylons, cables, and piers can be expressed as follows

$$D_{pyst} = \frac{1}{2}\rho U_z^2 C_{pyD} B_{py}\,;\;\; D_{cst} = \frac{1}{2}\rho U_z^2 C_{cD} B_c\,;\;\; D_{pst} = \frac{1}{2}\rho U_z^2 C_{pD} B_p \tag{7}$$

where C_{pyD}, C_{cD}, C_{pD} are the drag force coefficients of pylons, cables, and piers, respectively; B_{py}, B_c and B_p are the width of pylons, cables, and piers, respectively.

Different from the bridge deck which has small elevation change, the elevations of pylons, cables, and piers can vary significantly so that the altitude gradient of the mean wind should be also introduced correspondingly. It is assumed that the vertical wind velocity follows a power law relationship (Simiu and Scanlan 1996). So, the mean velocity along pylons, cables, and piers can be determined according to the mean velocity of the bridge deck elevation at the mid-span.

3.3 Buffeting forces acting on the whole bridge

The modified spectral representation method discussed earlier allows that the simulated points have different spacing and different elevation. Thus, the wind field simulation points in this study are chosen to be coincided with the discrete nodes of the bridge FEM model. As a result, it is convenient to derive the buffeting force acting on the element directly according to the turbulent wind velocities at the element nodes.

The buffeting forces for a unit span in the vertical, lateral, and torsional directions on the center of bridge elasticity can be expressed as follows (Scanlan 1978).

$$\mathbf{P}_b = \begin{Bmatrix} L_b(t) \\ D_b(t) \\ M_b(t) \end{Bmatrix} = 0.5\rho U_z \left(B_d \begin{Bmatrix} 2C_L(\theta) \\ 2C_D(\theta) \\ 2B_d C_M(\theta) \end{Bmatrix} u(t) + B_d \begin{Bmatrix} C_L^{'}(\theta) + C_D(\theta) \\ C_D^{'}(\theta) \\ B_d C_M^{'}(\theta) \end{Bmatrix} w(t) \right) = 0.5\rho U_z (\mathbf{C}_{bu} u(t) + \mathbf{C}_{bw} w(t)) \tag{8}$$

where $C_L^{'}(\theta) = dC_L/d\theta$, $C_D^{'}(\theta) = dC_D/d\theta$,and $C_M^{'}(\theta) = dC_M/d\theta$; $u(t)$ and $w(t)$ are the horizontal and vertical components of the turbulent wind velocities, respectively.

When a structural element is small enough, it can be assumed that the longitudinal and vertical wind fluctuations acting on the element are distributed linearly. The wind velocity components in both the longitudinal and vertical directions can be determined by the turbulent wind velocities of the two nodes of the element, respectively as

$$u(t) = \begin{bmatrix} 1-\dfrac{x}{L} & \dfrac{x}{L} \end{bmatrix} \begin{Bmatrix} u_1(t) \\ u_2(t) \end{Bmatrix} \mathbf{Au}^e \tag{9a}$$

$$w(t) = \begin{bmatrix} 1-\dfrac{x}{L} & \dfrac{x}{L} \end{bmatrix} \begin{Bmatrix} w_1(t) \\ w_2(t) \end{Bmatrix} \mathbf{Aw}^e \tag{9b}$$

where x and L are the axial location and the length of the element, respectively; and the subscripts 1 and 2 indicate the two ends of the element; $u_1(t), w_1(t)$ and $u_2(t)$, $w_2(t)$ are the longitudinal and vertical wind fluctuations of the two ends of the element, respectively.

The consistent buffeting forces at the element ends in the local coordinate system can be obtained by the following integration:

$$\mathbf{F}_b^e = \int_L \mathbf{B}^T \mathbf{P}_b dx \ = 0.5\rho U (\int_L \mathbf{B}^T \mathbf{C}_{bu} \mathbf{A} dx \mathbf{u}^e + \int_L \mathbf{B}^T \mathbf{C}_{bw} \mathbf{A} dx \mathbf{w}^e) \ = 0.5\rho U (\mathbf{A}_{bu}^e \mathbf{u}^e + \mathbf{A}_{bw}^e \mathbf{w}^e) \tag{10}$$

where $\mathbf{A}_{bu}^e$ and $\mathbf{A}_{bw}^e$ are the buffeting force matrices of the element corresponding to the longitudinal and vertical wind fluctuations, respectively; and B is the matrix of interpolated functions.

The matrices $\mathbf{A}_{bu}^e$ and $\mathbf{A}_{bw}^e$ can be derived as

$$\mathbf{A}_{bu}^e = \frac{-B_d L}{30} \begin{bmatrix} 0 & 21C_L(\theta) & 21C_D(\theta) & 20BC_M(\theta) & -3LC_D(\theta) & 3LC_L(\theta) \\ 0 & 9C_L(\theta) & 9C_D(\theta) & 10BC_M(\theta) & -2LC_D(\theta) & 2LC_L(\theta) \end{bmatrix.$$
$$\left. \begin{matrix} 0 & 9C_L(\theta) & 9C_D(\theta) & 10BC_M(\theta) & 2LC_D(\theta) & -2LC_L(\theta) \\ 0 & 21C_L(\theta) & 21C_D(\theta) & 20BC_M(\theta) & 3LC_D(\theta) & -3LC_L(\theta) \end{matrix} \right]^T \tag{11}$$

$$\mathbf{A}_{bw}^e = \frac{-B_d L}{60} \begin{bmatrix} 0 & 21(C_L^{'}(\theta) + C_D(\theta)) & 21C_D^{'}(\theta) & 20B_d C_M^{'}(\theta) & -3LC_D^{'}(\theta) & 3L(C_L^{'}(\theta) + C_D(\theta)) \\ 0 & 9(C_L^{'}(\theta) + C_D(\theta)) & 9C_D^{'}(\theta) & 10B_d C_M^{'}(\theta) & -2LC_D^{'}(\theta) & 2L(C_L^{'}(\theta) + C_D(\theta)) \end{bmatrix.$$
$$\left. \begin{matrix} 0 & 9(C_L^{'}(\theta) + C_D(\theta)) & 9C_D^{'}(\theta) & 10BC_M^{'}(\theta) & 2LC_D^{'}(\theta) & -2L(C_L^{'}(\theta) + C_D(\theta)) \\ 0 & 21(C_L^{'}(\theta) + C_D(\theta)) & 21C_D^{'}(\theta) & 20BC_M^{'}(\theta) & 3LC_D^{'}(\theta) & -3L(C_L^{'}(\theta) + C_D(\theta)) \end{matrix} \right]^T \tag{12}$$

The local nodal buffeting forces can be converted into the global coordinate system using the coordinate transformation matrix. As a result, the global nodal buffeting force vector can be obtained as

$$\mathbf{F}_b = 0.5\rho U (\mathbf{A}_{bu} \mathbf{u} + \mathbf{A}_{bw} \mathbf{w}) \tag{13}$$

where $\mathbf{A}_{bu}$ and $\mathbf{A}_{bw}$ are the global buffeting force matrices; and **u** and **w** are the r-row nodal fluctuating wind vectors for the longitudinal and vertical components, respectively. r is the number of nodes subjected to wind fluctuations.

Similar to the bridge deck, the buffeting forces on the bridge pylons, cables, and other components can be determined. Thus, the buffeting loading of the whole bridge can be considered. Typically, only buffeting drag forces are considered for pylons, cables, and piers, with their buffeting forces per unit length being expressed as follows.

$$D_{pyb} = \rho U_z C_{pyD} B_{py} u(t)\,;\quad D_{cb} = \rho U_z C_{cD} B_c u(t)\,;\quad D_{pb} = \rho U_z C_{pD} B_p u(t) \tag{14}$$

3.4 Self-excited forces

To investigate the aerodynamic stability of long-span suspension bridges, Lin (1987) expressed the self-excited forces in terms of convolution integrals between the bridge deck motion and the impulse response function. This procedure is adopted in the present study and is briefly summarized as follows (Bucher and Lin 1987, Ding and Lee 2000). Firstly, the self-excited forces in terms of convolution integrals between the bridge deck motion and the impulse response function in the time domain are expanded to incorporate the vertical, lateral, and rotational motions; secondly, the Fourier transformation is conducted and the rational function (Bucher and Lin 1987) is introduced to achieve the approximate expressions of a non-steady aerodynamic transfer function; then, the flutter derivatives measured from the wind tunnel are used to obtain the non-dimensional coefficients of the non-steady aerodynamic transfer function by the least squares curve-fitting method; finally, the self-excited lift, drag and moment acting on per unit length of the bridge deck are derived as follows.

$$\begin{bmatrix} 0 \\ L_{se}(t) \\ D_{se}(t) \\ M_{se}(t) \\ 0 \\ 0 \end{bmatrix} = \begin{bmatrix} 0 \\ F(\mathbf{C}_{Lh}, h, t) + F(\mathbf{C}_{Lp}, p, t) + B_d F(\mathbf{C}_{L\alpha}, \alpha, t) \\ F(\mathbf{C}_{Dh}, h, t) + F(\mathbf{C}_{Dp}, p, t) + B_d F(\mathbf{C}_{D\alpha}, \alpha, t) \\ B_d F(\mathbf{C}_{Mh}, h, t) + B_d F(\mathbf{C}_{Mp}, p, t) + B_d^2 F(\mathbf{C}_{M\alpha}, \alpha, t) \\ 0 \\ 0 \end{bmatrix} \tag{15}$$

where h, p, α are the vertical, lateral and torsional displacements of the bridge deck, respectively; $F(\mathbf{C}_{rx}, x, t)$ (r = D, L, or M; x = h, p, or α) are the components of the self-excited lift, drag and moment due to the vertical, lateral and torsional motion, which can be expressed as follows

$$F(\mathbf{C}_{rx}, x, t) = \rho U_z^2 \left[C_1 x(t) + C_2 \frac{B_d}{U_z} \dot{x}(t) + C_3 \int_0^t e^{-\frac{d_3 U_z}{B}(t-\tau)} \dot{x}(\tau) d\tau + C_4 \int_0^t e^{-\frac{d_4 U_z}{B}(t-\tau)} \dot{x}(\tau) d\tau \right] \tag{16}$$

where $C_x = \{C_1, C_2, C_3, d_3, C_4, d_4,\}^T$ are the uncertain coefficients corresponding to each component of the self-excited forces, which are functions of the flutter derivatives obtained from wind tunnel experimental studies. For example, the component of the self-excited moment $F(\mathbf{C}_{M\alpha}, x, t)$ can be expressed as

$$\begin{cases} \dfrac{C_1 v^2}{4\pi^2} + \displaystyle\sum_{k=3}^{n} \dfrac{C_k v^2}{d_k^2 v^2 + 4\pi^2} = A_3^*(v) \\ \dfrac{C_2 v}{2\pi} + \displaystyle\sum_{k=3}^{n} \dfrac{C_k d_k v^3}{2\pi d_k^2 v^2 + 4\pi^2} = A_2^*(v) \end{cases} \tag{17}$$

where A_2^* and A_3^* are the flutter derivatives, v is the reduced velocity, and the unknown coefficients $C_1 \ldots C_n$, $d_3 \ldots d_n$ can be obtained by the least squares curve fitting method.

3.5 Coupling relationships between vehicle and bridge

According to the determination method of the bridge displacement at the tire-bridge deck contact points, the coupling relationship of the vehicle-bridge interaction can be divided into the single-girder model and grillage model (Han 2014b). The single girder bridge model is generally used for long span bridges with box cross sections and the grillage method is more suitable for the cross section which is composed of several girders or steel truss section. For a vehicle traveling on a typical steel box girder, Fig. 1 shows the relationship between the tire-bridge deck contact points and a typical single-girder space beam element.

The vertical and lateral forces imposed by the left (right) wheel of the j th axle of the i th vehicle on the bridge deck can be expressed as

$$F_{ivzL(R)}^{j} = K_{vlL(R)}^{j}(Z_{vaL(R)}^{j} - Z_{bL(R)}^{j} - r_{L(R)}^{j}(x)) + C_{vlL(R)}^{j}(\dot{Z}_{vaL(R)}^{j} - \dot{Z}_{bL(R)}^{j} - \dot{r}_{L(R)}^{j}(x)) \tag{18a}$$

$$F_{ivyL(R)}^{j} = K_{ylL(R)}^{j}(Y_{vaL(R)}^{j} - Y_{bL(R)}^{j}) + C_{ylL(R)}^{j}(\dot{Y}_{vaL(R)}^{j} - \dot{Y}_{bL(R)}^{j}) \tag{18b}$$

where $K_{vlL(R)}^{j}$ and $K_{ylL(R)}^{j}$ are the lower vertical and lateral spring stiffness coefficient of the left (right) wheel, respectively; $C_{vlL(R)}^{j}$ and $C_{ylL(R)}^{j}$ are the lower vertical and lateral damping coefficient of the left (right) wheel, respectively; $Z_{vaL(R)}^{j}$ and $Y_{vaL(R)}^{j}$ are the vertical and lateral displacements of the left (right) wheel, respectively; a dot superscript "." denotes a differential with respect to time t; $\dot{r}_{L(R)}^{j}(x) = (dr_{L(R)}^{j}(x)/dx)\cdot(dx/dt) = (dr_{L(R)}^{j}(x)/dx \cdot U_v$ and U_v is the vehicle velocity; $Z_{bL(R)}^{j}$ and $Y_{bL(R)}^{j}$ are the vertical and lateral bridge deformations at the left (right) tire-bridge deck contacting points, respectively, which can be expressed as

$$Z_{bL(R)}^{j} = w_c + e_{L(R)}^{j}\theta_{xc}; \; Y_{bL(R)}^{j} = v_c + h_{L(R)}^{j}\theta_{xc} \tag{19}$$

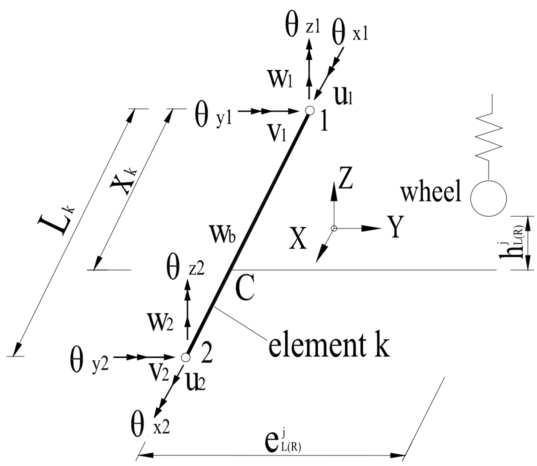

Fig. 1 The relationship between wheels and a typical single-girder space beam element.

where w_c, v_c and θ_{xc} are the vertical, lateral, and rotational deformation of point *C* in the bridge deck center which is located at the same cross section with the tire-bridge deck contact points. The displacements at the contact points can be determined from the nodes according to the interpolation relation of finite element method; $e^j_{L(R)}$ and $h^j_{L(R)}$ are the horizontal and vertical distances from the left (right) tire-bridge deck contact points to the deck center, respectively.

The vertical contact force distributed to the main girder is equal to the loads applied on the two discrete nodes of element k, and then the interaction forces on the bridge deck surface are determined for all the axles of all the vehicles traveling on the bridge as

$$\mathbf{F}^e_{bv} = \sum_{j=1}^{n_v}\sum_{i=1}^{n_a}\sum_{k=1}^{n_b}\Big[0 \quad F^j_{ivzL(R)}D_1D_2^2 \quad F^j_{ivyL(R)}D_1D_2^2 \quad \left(F^j_{ivzL(R)}e^j_{L(R)} + F^j_{ivyL(R)}h^j_{L(R)}\right)D_1D_2^2 \quad F^j_{ivyL(R)}x_kD_2^2 \quad F^j_{ivzL(R)}x_kD_2^2 \Big| \\ 0 \quad F^j_{ivzL(R)}D_3D_4^2 \quad F^j_{ivyL(R)}D_3D_4^2 \quad \left(F^j_{ivzL(R)}e^j_{L(R)} + F^j_{ivyL(R)}h^j_{L(R)}\right)D_3D_4^2 \quad -F^j_{ivyL(R)}x_kD_2D_4^2 \quad -F^j_{ivzL(R)}x_kD_2D_4^2\Big|\Big]^T \tag{20}$$

where n_b is the total number of vehicle lane element of the bridge; n_a is the axle number of a single vehicle; n_v =total number of vehicles on the bridge; $D_1 = 1 + 2x_k / L_k$, $D_2 = 1 - x_k / L_k$, $D_3 = 3 - 2x_k / L_k$, $D_4 = x_k / L_k$; x_k is the distance between the node 1 and node *C* of element k; and L_k is the length of element k.

3.6 Interactions between wind and vehicle

The wind-vehicle interaction is one of the most direct parameters influencing the safety and comfort of the vehicle. Wind action on a running vehicle includes static and dynamic load effects. The quasi-static wind forces on vehicles are adopted in this study since a transient type of force model is not yet available (Baker 1994). The total horizontal wind velocities acting on the vehicle comprise the mean wind velocity component and the turbulent wind velocity component. It is noted that the turbulent wind speed $u(x_v, t)$ acting on the vehicle is not only a function of time but also position because the instantaneous position of a moving vehicle is time-variant. The longitudinal fluctuating wind speeds impacting the vehicle should be compatible with the wind speeds used for determining the wind forces acting on the bridge deck. Therefore, if the position of the vehicle x_v at any time t is located between the node i and j of the bridge deck, the $u(x_v, t)$ will be used to determine wind forces on the vehicle, which is determined by

$$u(x_v, t) = \left(\frac{x_v - x_i}{x_j - x_i}\right)u_j(t) + \left(\frac{x_j - x_v}{x_j - x_i}\right)u_i(t) \tag{21}$$

where x_i and x_j are the x-coordinate of node i and node j, respectively; and $u_i(t)$ and $u_j(t)$ are the corresponding horizontal turbulent wind speed at a given time t.

3.7 Geometric and aerodynamic nonlinearities

As discussed earlier, geometric and aerodynamic nonlinearities have become more important for long-span cable-stayed bridges. The overall geometric and aerodynamic nonlinear behaviors mainly originate from: (1) the influence of cable sag on its equivalent modulus of elasticity; (2) the influence of initial stresses on structural stiffness; (3) the influence of large displacements on structural stiffness and loads; and (4) the attack angle effect of static and aerodynamic wind forces and nonlinear component of self-excited forces. The corresponding methods dealing with geometric and aerodynamic nonlinearities in this study are listed as follows: (1) an equivalent straight chord member with an equivalent modulus of elasticity, that combines the effects of both material and geometric deformations, is used to account for this variation in cable axial stiffness (Ernst 1965). (2) Analogous to that of cable elements, the stiffness of a beam element is composed of two parts: elastic stiffness and geometric stiffness. Based on the large displacement theory, a geometric stiffness matrix (Pan and Cheng 1994) of beam elements incorporating the contribution of the axial force and bending moments is adopted. (3) The nodal coordinates can be updated at the end of each time step to address large displacements. (4) Determine the effective wind attack angle of the bridge deck at each time step, and then the corresponding static and aerodynamic wind forces can be calculated by interpolation. (5) Nonlinear iteration method is used to deal with the nonlinearity of self-excited forces. It is noted that all the five nonlinearity treatments will be incorporated in the solution of the wind-traffic-bridge system discussed as follows.

4. Equation of motion of wind-traffic-bridge system and solution

There are mainly two different methods of assembling and solving the vehicle-bridge system or wind-vehicle-bridge system: one is that the vehicle and bridge equations are coupled together and solved by direct integration method (Chen and Cai 2007); the other one is that the vehicle and bridge equations are established independently and solved by a nonlinear iteration method (Yang and Fonder 1996, Li *et al*. 2005, Li *et al*. 2013, Han 2014b). The first one has the advantage of solving directly while the degree of freedom (DOF) of the coupled system is dependent on both the DOF of the bridge model and the number of vehicles on the bridge. When there is simultaneous presence of a high number of vehicles on the bridge, for a fully coupled interaction analysis of a wind-traffic-bridge system the number of degrees of freedom increases dramatically and may become unrealistic for practical simulations (Chen and Cai 2007, Chen and Wu 2010). The nonlinear iteration method can overcome the disadvantage of the direct integration method, because the bridge and vehicle systems are established individually so the DOF of two subsystems have nothing to do with each other. Therefore, the nonlinear iteration method is ideal for the simulation of a large amount of vehicles on the bridge deck simultaneously. Furthermore, when dealing with geometric and aerodynamic nonlinearities, the coupled systems of bridge and traffic under a certain wind excitations must be solved by the iteration approach because of its double nonlinearity of structure including geometric nonlinearity on the left side and load nonlinearity on the right side of the equation of the motion (Zhang *et al*. 2002).

The bridge and the vehicle are regarded as two subsystems and the equations of motion of the wind-traffic-bridge system can be expressed in the following form.

$$\mathbf{M}_b\ddot{u}_b+\mathbf{C}_b\dot{u}_b+\mathbf{K}_bu_b=\mathbf{F}_{bg}+\mathbf{F}_{bst}+\mathbf{F}_{bbu}+\mathbf{F}_{bse}+\mathbf{F}_{bv} \tag{22a}$$

$$\mathbf{M}_v\ddot{u}_v+\mathbf{C}_v\dot{u}_v+\mathbf{K}_vu_v=\mathbf{F}_{vg}+\mathbf{F}_{vst}+\mathbf{F}_{vb} \tag{22b}$$

where $\mathbf{M}, \mathbf{C}$ and $\mathbf{K}$ are the mass, damping and stiffness matrix, respectively; u represents the displacement vector; Subscripts v and b denote the vehicle and bridge, respectively; $\mathbf{K}_b$ can be divided into two components: elastic stiffness $\mathbf{K}_e$ and geometric stiffness $\mathbf{K}_g$, and $\mathbf{K}_b = \mathbf{K}_e + \mathbf{K}_g$; $\mathbf{F}_{bg}, \mathbf{F}_{bst}, \mathbf{F}_{bbu}, \mathbf{F}_{bse}$ and $\mathbf{F}_{bv}$ are the self-weight of the bridge, the static wind forces, buffeting forces, self-excited forces, and the wheel-bridge contact forces acting on the bridge, respectively; $\mathbf{F}_{vg}$, $\mathbf{F}_{vst}$ and $\mathbf{F}_{vb}$ are the self-weight of the vehicle, the quasi-static wind forces, and the wheel-bridge contact forces acting on the vehicle, respectively.

The bridge and vehicle subsystems are solved independently firstly, and then the two subsystems are coupled together through relative geometry relationships between the tire and the bridge deck at the contact points and the interaction forces. An iterative process is applied to ensure the displacement and force compatibility conditions to be satisfied at the tire-bridge deck contact points at each time step. The main procedures for nonlinear dynamic analysis of long-span bridges under the combined loads of traffic and wind are as follows (Han *et al*. 2011).

(1) Input basic data. Bridge: basic geometric and material parameters, bridge finite element model, surface roughness of the bridge deck. Traffic: vehicle classifications, vehicle occupancy and speed limit; Wind: wind speed, aerostatic and aerodynamic coefficients for the whole bridge and static wind force coefficients of various typical vehicles.

(2) Determine the static equilibrium position of the bridge under the dead load and the current mean wind speed *U*, and then perform the nonlinear three-dimensional vibration analysis of the bridge under the combined real traffic load and wind.

(3) Determine the number and positions of all vehicles traveling on the bridge and combine the road roughness and deck movements ($\ddot{u}_b^{\,t-1}, \dot{u}_b^{\,t-1}, u_b^{\,t-1}$) at the *t*-1 time step, yielding the vertical and lateral stimulus sources at the current t time step of each tire for all vehicles.

(4) The forces acting on each vehicle at the current time step induced by the vertical and lateral stimulus sources and the total equivalent horizontal wind forces are calculated.

(5) The vehicle subsystem in Eq. (22(b)) can be independently solved with the Newmark integration method to obtain the initial vehicle response ($\ddot{u}_v^{\,t}, \dot{u}_v^{\,t}, u_v^{\,t}$) at the current time step *t*.

(6) Solve the bridge responses at the current time step t.

(6.a) The tire-bridge deck interaction forces at the current time step *t* can be determined according to the obtained vehicle responses.

(6.b) The initial wind attack angles for the previous equilibrium state at the *t*-1 time step and corresponding wind tunnel test data are used to calculate the static and buffeting forces of bridge structure.

(6.c)The bridge responses ($\ddot{u}_b^{\,t-1}, \dot{u}_b^{\,t-1}, u_b^{\,t-1}$) at the last time step *t*-1 are regarded as the initial value and the self-excited forces of bridge corresponding to the initial wind attack angles at the current time step t can be obtained.

(6.d) The initial large displacement and internal forces at the *t*-1 time step are used to update structural geometry, equivalent modulus of elasticity and form geometric stiffness matrix, and then combine with the elastic stiffness matrix to form whole stiffness matrix of the left items of Eq. (22a). The load matrix of the bridge is formed and the bridge subsystem in Eq. (22(a)) can be independently solved by the Newmark integration method and the new deformed position and internal forces state are then obtained and updated.

(6.e) The effective wind attack angle of the deck, structural geometry, and internal forces state at the current time step t are regarded as the initial value for step (6.b), (6.c) and (6.d), respectively, and the steps from (6.b) to (6.e) are repeated until the error of the self-excited force are less than the allowable value.

(7) The deck movements obtained at the step (6) are adopted for step (3). The steps from (3) to (7) are repeated until the geometric and force compatibility conditions at the tire–bridge deck contact points are satisfied and then the calculations continue in the next time step.

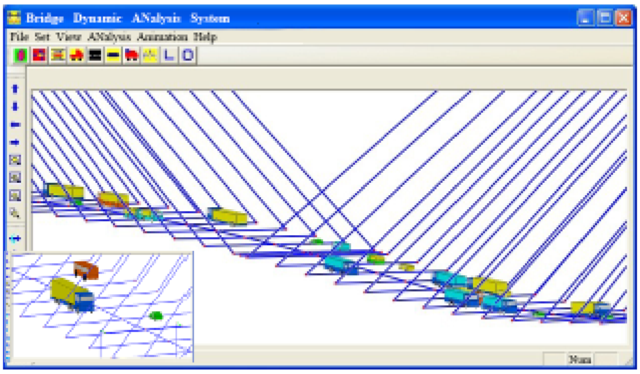

Fig. 2 Snapshot of traffic running on Sutong bridge in BDANS

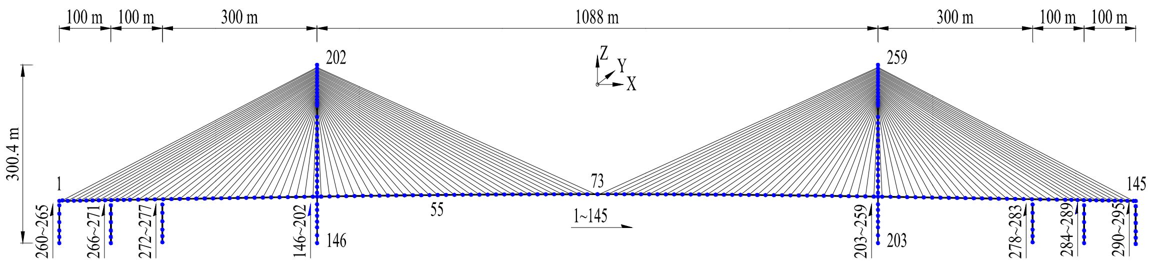

(a) Structural arrangement and positions of the simulation points.

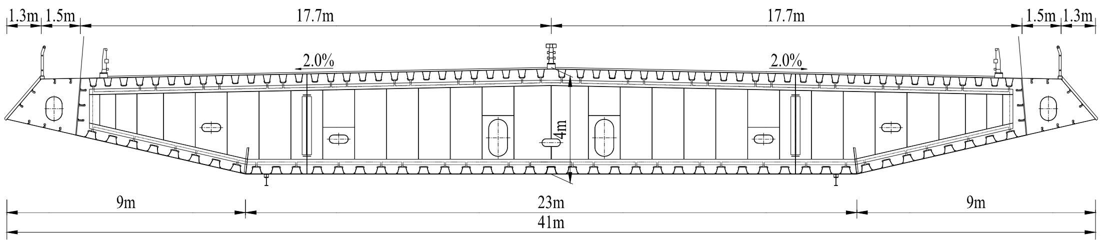

(b) Cross section of bridge deck

Fig. 3 Configuration of the Sutong Bridge

According to the above steps, the in-house software BDANS (Bridge Dynamic ANalysis System) is developed by the corresponding author of this paper with FORTRAN language. The interface of BDANS written by VC++ is shown in Fig. 2. Firstly, the FEM model of the bridges established by ANSYS can be imported into BDANS. Then, the information of vehicle and wind can be input and processed by BDANS. Finally, the responses of both the bridge and vehicle under wind excitations at any single time step during the process of vehicles' driving across the bridge can be calculated and displayed.

5. Case study

5.1 Bridge information

The Sutong Bridge is a box-girder cable-stayed bridge with a span arrangement of 100+100+300+1088+300+100+100 m. As shown in Fig. 3, the cross section adopts the streamlined, closed flat box girder, with a width of 41.0 m and height at the centerline of 4.0 m. Sutong bridge has double plane cables and twin towers. The stay cables are composed of parallel steel-wire strands. The intervals of these cables are 16 m at the main span, 12 m at the side spans, and 2 m along the towers. There are 272 stay cables in total and the length of the longest one is 577 m with the corresponding size of PES7-313. The main tower is 297.7 m high and in inverse-Y shape, including upper, middle, and bottom columns with a tie beam between the legs. Regarding the dynamic features of the Sutong Bridge, the basic frequency is 0.06221, corresponding to the mode shape of the longitudinal floating vibration of the steel box girder.

5.2 Stochastic wind velocity for the whole bridge

The modified spectral representation method discussed previously is used to simulate the whole bridge wind field for the Sutong Bridge and the wind speed distributions of the simulated points are shown in Fig. 3(a). The simulated points are chosen to coincide with the discrete nodes of the bridge finite element model. As a result, it can produce turbulent wind velocities at two end nodes of elements, based on which the buffeting forces acting on each element can be decided directly according to Eq. (10). There are 295 points distributed in the whole bridge in total, 145 points along the bridge deck axis considering longitudinal slope, 57 points distributed along each pylon and 6 points distributed along each pier.

The horizontal wind spectra adopted Kaimal's form (1972) while the vertical spectrum is in the form presented by Lumley and Panofsky (1964)

$$\frac{nS_{uu}(n)}{u_*^2} = \frac{200f}{(1+50f)^{5/3}} \tag{23}$$

$$\frac{nS_{ww}(n)}{u_*^2} = \frac{3.36f}{1+10f^{5/3}} \tag{24}$$

where f is dimensionless frequency; u_* is shear velocity in m/s; and n is frequency in Hz.
In the above equations

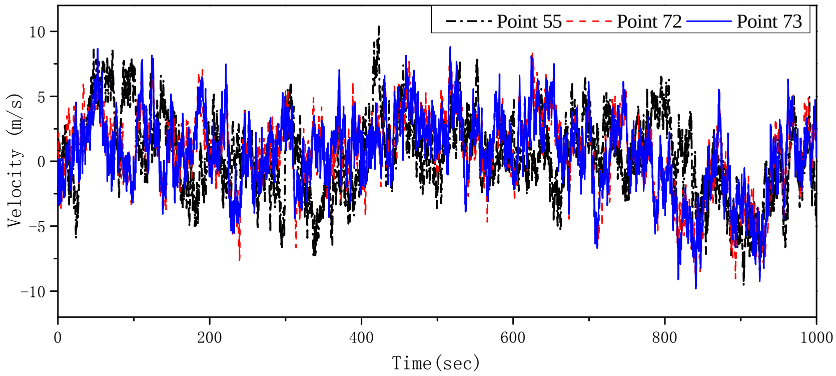

Fig. 4 Simulated wind velocities at points 55, 72, and 73

$$f = \frac{nz}{U(z)} \quad , u_* = \frac{KU(z)}{\ln(\frac{z}{z_0})} \tag{25}$$

where $U(z)$ is mean longitudinal wind velocity in m/s at height z; z_0 is the ground roughness length in meters and K is Von Karman constant and usually set as 0.4.

The coherence function adopted in Davenport's form (1968) is in following form

$$coh(r,\omega) = \exp(-\frac{\omega}{2\pi}\frac{[C_z^2(z_1-z_2)^2 + C_y^2(y_1-y_2)^2]^{1/2}}{\frac{1}{2}[U(z_1)+U(z_2)]}) \tag{26}$$

where ω is frequency in rad/s, y_1, y_2 and z_1, z_2 are the longitudinal and vertical coordinates corresponding to two spatial simulated points 1 and 2, respectively; C_z and C_y are the longitudinal and vertical decay factors related to wind correlation, respectively, and the values of which are suggested as 7 according to MTPRC(2004); $U(z_1)$ and $U(z_2)$ are the mean longitudinal wind velocity in m/s at the height z_1 and z_2, respectively.

The main parameters are as follows: the height of the deck above ground z=55.4 m; the ground roughness z_0 = 0.01 m; the average wind velocity on the deck $U(z)$ = 15.0 m/s; the upper cutoff frequency $\omega_{up} = 4\pi$ rad/s; the dividing number of frequency N = 2048; the time interval dt = 0.1 s; the period T_0 = 4096s, and the target wind spectrum is Kaimal's spectrum.

The Deodatis and modified Deodatis methods are both used to simulate the longitudinal and vertical fluctuating wind velocity profiles of all the wind simulated points at the same time. Only 296 frequency points are conducted in the Cholesky decomposition when the modified Deodatis method is used. While it takes 149.6 minutes and 98. 3MB computer memory to carry out the whole bridge wind field simulation using Deodatis method, it only takes 3.7 minutes and 10. 6MB memory cost to conduct the same simulation after the interpolation technique is introduced in the modified Deodatis method. Therefore, the modified Deodatis method implemented in the present study can improve the calculation efficiency greatly and demand less memory cost.

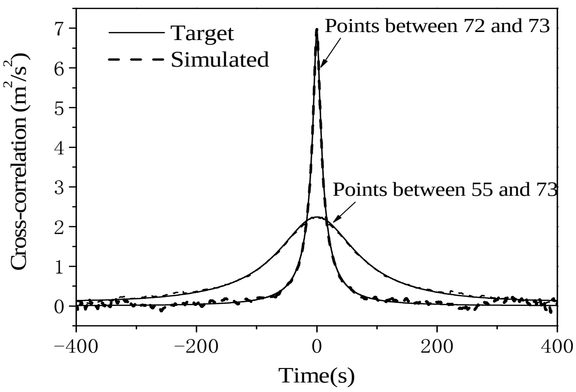

(a) Correlation functions

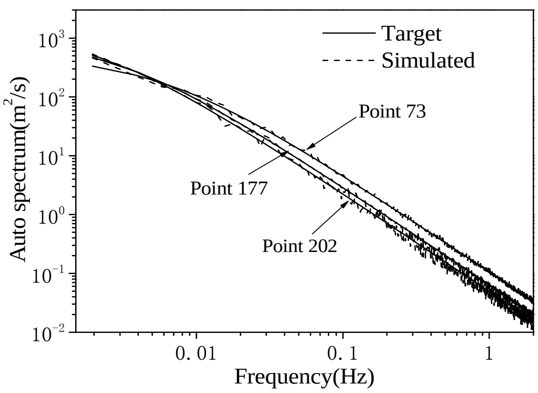

(b) Auto-spectrum S_u

Fig. 5 Comparison of simulated and target results

Fig. 4 illustrates the correlation between the fluctuating vertical wind velocity profile for Point 55(around quarter main span), Point 72(near the mid-span), and Point73 (mid-span) along the bridge deck, respectively. From the figure it can be seen that the turbulent wind profiles for Points 72 and 73 have very strong correlation, whereas the correlation is much weaker between Point 55 and Point 73 because they are far away compared the distance between Point 72 and Point73. Fig. 5(a) compares the simulated and target correlation functions of the fluctuating velocities between Point 55 and Point 73 and between Point 72 and Point 73. It is found that the simulated correlation functions agree well with the target ones.

5.3 Aerostatic and aerodynamic parameters for bridge

Section model test (Chen and Ma 2004) was carried out in the wind tunnel at Tongji University to obtain the aerostatic and aerodynamic coefficients of the bridge deck. Eight vertical and torsional flutter derivatives of the bridge deck were identified and the flutter derivatives of the Sutong Bridge are curve-fitted following Eq. (17) and displayed in Fig. 6 (e.g., $A_1^*, i = 1,2,3,4$). Sectional model tests were also conducted to measure the aerostatic forces and the model scaling factor is 1:70. The wind attack angle is from -10^o to +10^o and the angle interval is 1^o. Fig. 7 presents the bridge deck aerostatic coefficients at various angles of wind incidence. The whole pylon can be divided into three parts according to the aerodynamic shape, that is, the upper, middle and lower columns. The drag coefficients of these three typical columns can be calculated by discrete vortex method (Chen *et al*. 2005). The drag coefficient of the upper column is 1.69, the windward and leeward drag coefficients of the middle columns are 1.41 and 0.34, respectively, and the windward and leeward drag coefficients of the bottom columns are 1.53 and 0.60, respectively. The experiments for the cable drag coefficient were carried out through wind tunnel strain-gauge balance in the smooth flow and it was found that the drag coefficient is 0.8 (Chen and Ma 2005) and the drag coefficient of pier is 1.4 (Xiang *et al*. 2004).

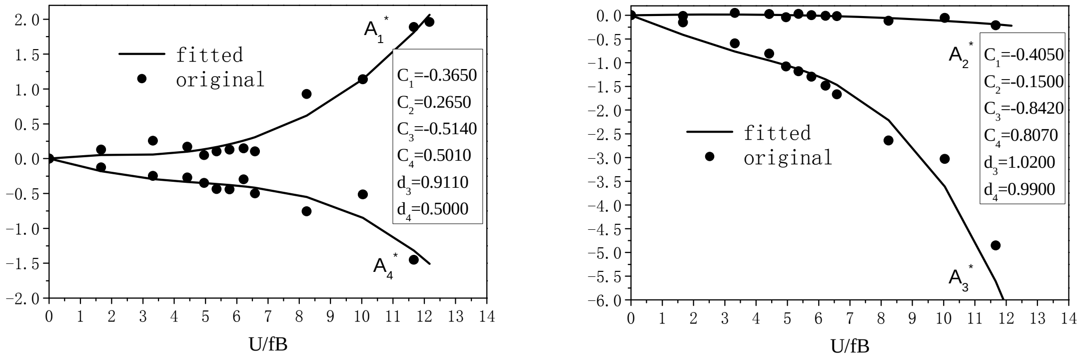

Fig. 6 Measured and Fitted flutter derivatives

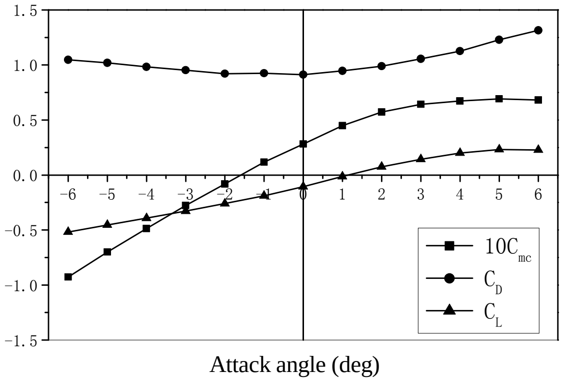

Fig. 7 Aerostatic coefficients of the bridge deck

5.4 Traffic flow simulation results

The cellular automation (CA) traffic flow simulation model is used to simulate the stochastic traffic flow traveling on the super long cable-stayed bridge, among which each vehicle carries detailed time-variant information such as the instantaneous driving speed and position at each time step as well as time-invariant information (e.g., vehicle type and vehicle weight). Since the main concern of this study is the establishment of nonlinear analysis framework of the wind-traffic-bridge system that considers the wind forces acting on the whole bridge, only three typical vehicle types are incorporated in the simulation to present the proposed analysis model. A vehicle occupancy corresponding to smooth traffic (15veh/mile/lane) is chosen and the three typical vehicle models are heavy multi-axle truck, high-sided truck, and sedan car. All the basic parameters of the traffic flow simulation, the parameters of the three vehicle models and corresponding wind force coefficients are the same as that used by Chen and Wu (2010). Due to the page limitation, Fig. 8 shows the simulated traffic snapshot on the opposite two-way 6 lanes at the time of 100s and only 200 meters long bridge deck simulation results are chosen.

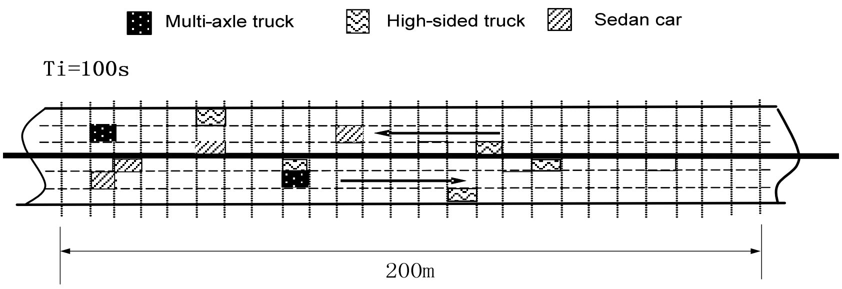

Fig. 8 CA-based traffic flow simulation result

5.5 Dynamic response of bridge

To have a better view of the effect of the whole bridge wind fields on the responses of the bridge, two different wind field simulation methods are chosen in the following analysis: one is the simulation of correlated wind fields on bridge deck only and the other one is the simulation of wind fields on the whole bridge. Fig. 9 shows the simulated vertical and lateral displacement time histories at the mid-span of the bridge girder at the mean velocity of 10 m/s and 20 m/s under two different wind field models. Furthermore, the corresponding responses of the traffic-bridge analysis without wind are also drawn together for comparisons.

Based on the observations from Fig. 9, the characteristics of bridge's dynamic performance under random traffic flow and wind loads are summarized as follows:

1) The vertical displacements corresponding to 10 m/s wind slightly oscillate about the ones under the stochastic traffic without wind. When the wind speed is 20 m/s, the bridge vertical displacement deviates significantly from the vertical deflection curve of traffic-bridge system. Therefore, it can be concluded that the bridge motion is dominated by the action of random traffic flow under low wind velocities, however, for higher wind velocities, the bridge motion is dominated by the excitation of wind force rather than the traffic flow.

2) Compared with the case of considering wind field of bridge deck only, considering the whole bridge wind field has almost no effect on the bridge vertical deflections whereas it increases the bridge lateral displacement significantly.

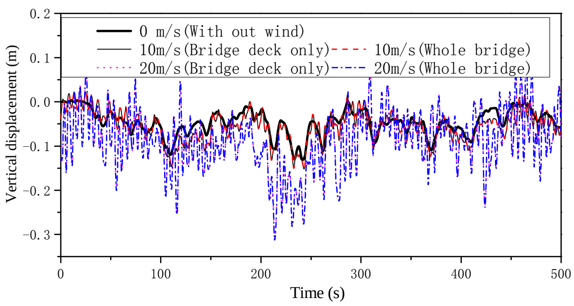

(a) Vertical displacement

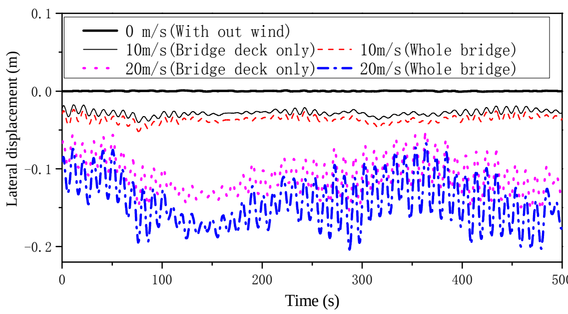

(b) Lateral displacement

Fig. 9 Displacement responses histories of bridge girder at mid-span

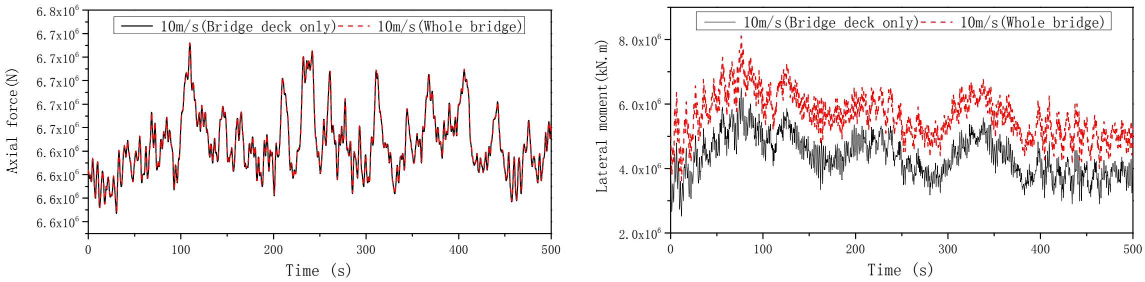

(a) Axial force of the longest cable (b) Lateral moment at the bottom of tower

Fig. 10 Internal force responses histories of key sections of the bridge

Regarding the responses output for wind-vehicle-bridge analysis, when the mode superposition approach is employed, modal analysis for the whole bridge including all components is conducted firstly, then the modal analysis results of interested component of bridge are selected for further analysis. For example, if only the results of the bridge girder are the main concern, the information of the bridge girder is extracted while other components such as bridge tower and cable are ignored. Compared with the mode superposition approach, the direct FEM method adopted in this study has one great advantage that the time history of displacement and internal forces at any node or any element of all the bridge components (girder, pylons and cables) can be directly obtained. Fig. 10 shows the time history of simulated axial force of the longest cable and lateral moment at the bottom of tower at the mean velocity of 10m/s under the above two different wind field models.

It can be seen from Fig. 10 that the consideration of the whole bridge wind field has almost no effect on the axial force of cable whereas it increases the lateral moment of bridge tower significantly.

In order to show the difference, the statistics of the bridge lateral displacement, acceleration and moment at the mid-span and lateral moment at the bottom of tower with two different wind field models are compared in Fig. 11. It can be seen from Fig. 11 that all the statistical indices of the bridge lateral response considering the whole bridge wind field are larger than those considering only the bridge deck wind field. Taking the maximum values of the lateral displacement and acceleration as an example, the calculated results considering the whole bridge wind field are 22.4%-33.5% and 26.3%-32.7% larger than the corresponding results considering only the bridge deck wind field, when the mean velocity of the turbulent wind is 0-25 m/s. Therefore, the neglect of wind forces acting on the pylons, cables, and piers may underestimate the responses of the bridge with unsafe results.

5.6 Dynamic response of vehicles

There are two main lateral excitation sources for vehicles traveling on the bridge deck in wind environments: one is the wind forces acting directly on the vehicle body and the other one is the bridge lateral motion transmitted through the tire-bridge contact point to the vehicle body (Cai and Chen 2004, Xia *et al*. 2008). While the whole bridge wind field will increase bridge lateral response significantly as discussed earlier, whether the amplified lateral motion of the bridge deck can strengthen the interaction between the bridge and the vehicle is still not clear, which will be investigated in the following part.

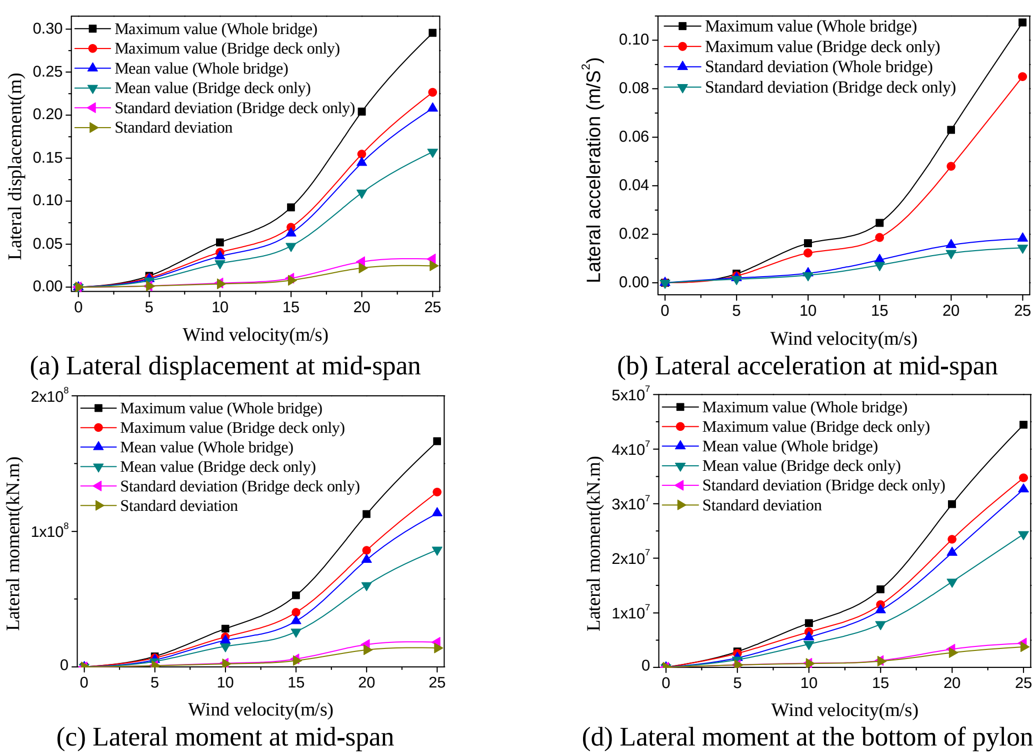

Fig. 11 Comparisons of lateral bridge displacements, accelerations and internal forces under two different wind models

A high-sided vehicle at the windward outermost lane is selected in the following analysis. The wind velocity profile acting on the vehicle is determined using the wind velocity dynamic interpolation technique proposed in Eq. (21) when the mean wind speed is 20 m/s. “Excellent” road roughness corresponding to class “A” defined in ISO (1972) is considered since the Sutong bridge is relatively new constructed.

The vertical and lateral interaction forces between the vehicle and the bridge are the key indices for vehicle overturning accident and sideslip accident, respectively (Baker 1994, Chen and Cai 2004), which act on the axle set and the bridge deck surface. The main procedures of the determination of the interaction forces are as follows. Firstly, the displacement, velocity, and acceleration of the vehicle including all rigid bodies and all the nodes of the bridge finite element model can be extracted directly from the numerical analysis model as proposed in this study. Secondly, the bridge displacement and velocity at the position of each tire-bridge contact point can be determined from the nodal information by locating the position of vehicle tire at different time instant. Finally, the vertical and lateral interaction forces can be determined from the relative motion of the axle set of the vehicle and the contact points of the bridge deck by Eq. (18). One typical axle set (left rear axle set) is selected as an example and the vertical and lateral bridge displacements at the contact points are plotted against with the corresponding displacements of the lower axle set in Figs. 12(a) and 12(b). As discussed earlier, the wind simulation model has almost no effect on the vertical responses of the bridges. Therefore, the vertical displacements of the lower axle set and contact points at the bridge deck are identical for both cases, showing nearly no effect on the vertical interaction forces from applying the whole bridge wind field (Fig. 12(a)). As shown in Fig. 12(b), the lateral displacements at the contact points corresponding to the whole bridge wind field are found to be considerably larger (about 18.7%) than those of the bridge deck wind field only. Therefore, it can be concluded that the whole bridge wind field model is important to the prediction of vehicle lateral displacements.

5.7 Influences of geometric and aerodynamic nonlinearities

The lateral interaction forces between the vehicle and the bridge deck are depicted in Fig. 13(a). It can be found that although the whole bridge wind field will increase the lateral displacements of the bridge and the vehicle system, the lateral sideslip forces under the two different wind models are almost identical. The lateral acceleration of the vehicle body is the key parameter for lateral driving comfort assessment, which is plotted in Fig. 13(b). It can be found from Fig. 13(b) that the wind field models have almost no effect on the lateral acceleration, the reason for which may be that the bridge vibration is kind of low-frequency vibration and the contribution of the lateral bridge vibration to the vehicle acceleration is very limited. Compared with the excitation source of the lateral motion from the bridge, the wind force acting directly on the vehicle body seems to play a dominant role on the vehicle lateral driving comfort and lateral interaction force

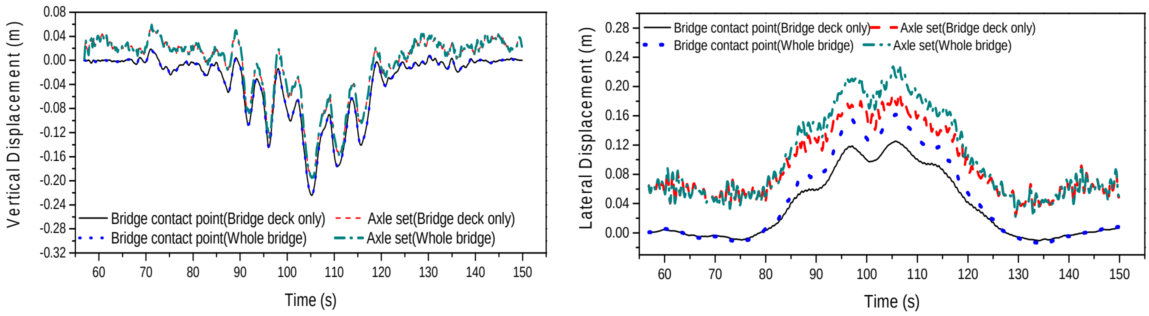

(a) Vertical displacement information at contact points (b) Lateral displacement information at contact points

Fig. 12 Comparisons of displacement information at contact points under two different wind models

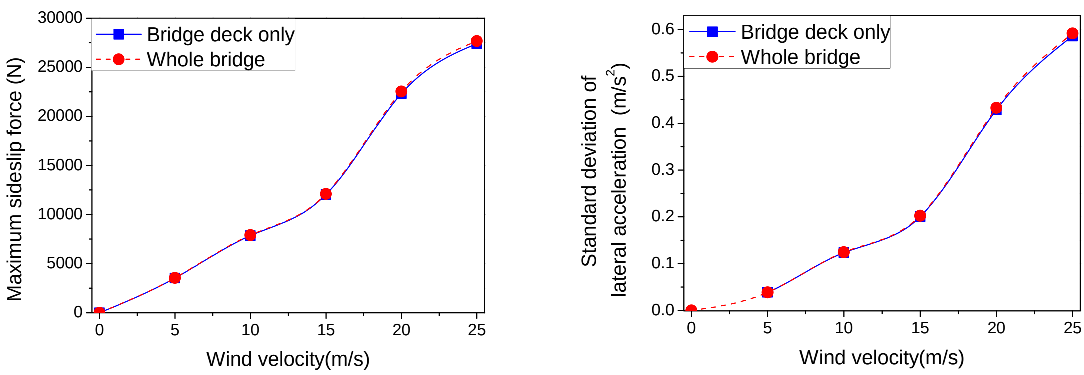

(a) Maximum sideslip force (b) Standard deviation of lateral acceleration

Fig. 13 Comparisons of lateral responses of the vehicle under two different wind models

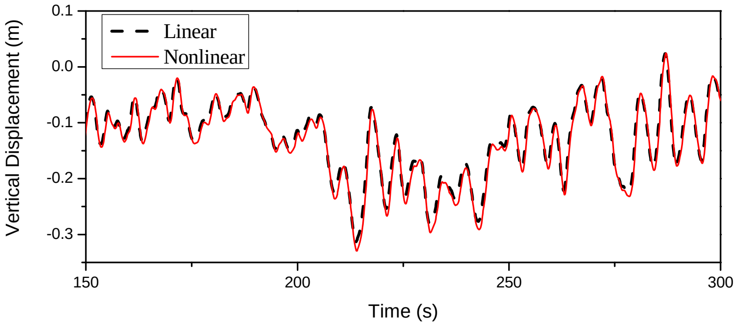

Fig. 14 Displacement response histories of bridge girder at mid-span

Table 1 Comparisons of linear and nonlinear maximum responses

Responses			A: Linear	b: Nonlinear	$\frac{\lvert B-A \rvert}{A} \times 100\%$
Bridge (mid-span)	Disp (m)	Vertical	0.3128	0.3252	3.98
		Lateral	0.2040	0.2020	-0.98
	Acce (m/s^2)	Vertical	0.2849	0.2764	-2.99
		Lateral	0.0630	0.0621	-1.48
Vehicle	Disp (m)	Vertical	0.1949	0.2007	2.96
		Lateral	0.2888	0.2865	-0.78
	Acce (m/s^2)	Vertical	0.9492	0.9460	-0.34
		Lateral	1.4890	1.4930	0.27
	Lateral force (N)		22320	22570	1.12

In order to investigate the effects of the geometric and aerodynamic nonlinearities on the vehicle-bridge system under wind action, nonlinear analysis is conducted under the wind velocity of 20 m/s and the comparisons with the linear analysis are shown in Fig. 14 and Table 1.

Some findings can be drawn from Fig. 14 and Table 1:

1) The maximum vertical bridge displacement at the mid-span of nonlinear analysis is about 3.98% larger than that of linear analysis. Furthermore, the wave peak and trough of the time history considering nonlinearities lag behind (Fig. 14) those corresponding to linear analysis. The reason is that the pylons and bridge deck of cable-stayed bridges withstand mainly compression with the geometric stiffness being negative, which will reduce structure stiffness and increase vibration period to some extent.

2) The nonlinear maximum vertical and lateral bridge accelerations at the mid-span are a little smaller than those of linear analysis. This can also contribute to the decrease of the vibration frequency considering nonlinearities and the level of vibration drops.

3) Consideration of nonlinear effects has very slight influence on the vehicle responses and the maximum error is no more than 3%. In general, the nonlinearities have slight influence on the responses of the bridge and vehicles. This is primarily because the wind speed considered is not high when traffic is also considered on the bridge.

In order to investigate the effects due to geometric and aerodynamic nonlinearities on the bridge buffeting responses without traffic, a high wind speed (70 m/s) is selected to conduct both linear and nonlinear time domain buffeting analysis. It is noted that the flutter critical wind speed observed in the full bridge aeroelastic model test of the Sutong bridge at $+3^{o}$ attack angle is 88.4 m/s (Chen *et al*. 2005).

Table 2 shows the comparisons of the root mean square (RMS) values at mid-span corresponding to linear and nonlinear analysis. As observed from Table 2, it is found out that the vertical and torsional displacements obtained from nonlinear analysis are 18.9% and 10.3% greater than those from linear analysis, respectively. However, the lateral displacements under the two cases are almost identical. Therefore, the geometric and aerodynamic nonlinearities have significant influence on the vertical and torsional displacements while they have a small effect on the lateral displacement.

For the dynamic simulation of long-span bridges under the combined loads of stochastic traffic and wind, the calculation efficiency is a crucial factor. In most existent wind-vehicle-bridge analysis, only one or several vehicles distributed in assumed patterns on the bridge are considered. Chen (2010) and Han (2011) firstly established the computational framework for long-span bridges under wind and stochastic traffic loads based on the mode superposition, and the direct FEM method respectively. However, the mode superposition method has limitations compared with the discrete FEM method as stated in the previous part. According to Chen and Wu's (2010) study, when a long-span cable-stayed with a total length of 836.9 m was selected as the prototype bridge and the smooth traffic (15veh/mile/lane) is adopted, the time and memory cost of the fully coupled wind-vehicle-bridge interaction analysis will be prohibitively high. They adopted a simplified method, i.e., equivalent wheel load approach, which will also take about 2 h to conduct 5-min simulation on a common personal computer. Compared with Chen and Wu's analytical framework, the framework adopting nonlinear iterative solution method presented in this paper is very efficient on the coupled analysis between the bridge and a large number of vehicles in wind environment. When the smooth traffic (15veh/mile/lane) is considered in this study, there are approximately 20 vehicles distributed in each lane (totally 6 lanes) for the whole bridge. With totally 120 vehicles simultaneous presence on the bridge at a given time, it takes a typical personal computer 11.3 minutes and 16.3MB memory to conduct linear analysis of the wind-traffic-bridge system, and 16.7 minutes and 19.4MB memory to conduct a nonlinear analysis.

Table 2 Linear and nonlinear RMS responses of bridge girder at mid-span

RMS	A: Linear	b: Nonlinear	$\frac{\lvert B-A \rvert}{A}\times 100\%$
Vertical(m)	0.684	0.813	18.9
Lateral(m)	0.383	0.388	1.2
Rotational(^{o})	0.370	0.408	10.3

Therefore, the nonlinear analysis framework adopting nonlinear iteration solution method presented in this paper can be used to conduct complex nonlinear fully coupled analysis with high computation efficiency and relatively low computational costs, which can fully satisfy the need of typical engineering analyses.

6. Conclusions

A three-dimensional nonlinear analysis framework of wind-traffic-bridge systems has been developed in this paper. The proposed analysis framework is applied to the Sutong Bridge and the influences of the whole bridge wind field model and geometric and aerodynamic nonlinearities on the responses of the wind-traffic-bridge system are discussed, some conclusions can be drawn as follows:

(1) The consideration of the whole bridge wind field has little effect on the bridge vertical responses, but considerable amplification on the bridge's lateral responses. Therefore, neglecting wind forces on the pylons, cables, and piers may underestimate the lateral responses of the bridge.

(2) While considering the whole bridge wind field has significant effect on the vehicle lateral deflection, it has nearly no effect on the lateral acceleration and the sideslip force of the vehicle. Compared with the lateral excitation from the bridge, the lateral wind force acting directly on the vehicle body was found to play a dominant role on the vehicle lateral acceleration and lateral interaction force.

(3) The geometric and aerodynamic nonlinearities have slight effect on the responses of the bridge and the vehicle system when the wind speed is not very high. For a wind velocity of 20 m/s, the maximum nonlinear vertical bridge displacement at the mid-span is about 3.98% larger than that of linear analysis and the wave peak and trough of the time history considering nonlinearities lag behind those corresponding to linear analysis. The maximum nonlinear vertical and lateral bridge accelerations at mid-span are a little smaller than those of linear analysis.

(4) In the present study, nonlinear analysis takes about 1.51 times the computational time of linear analysis. Therefore, depending on the requirement of accuracy or efficiency, nonlinear analysis or linear analysis can be chosen when the wind-traffic- bridge interaction is conducted. The proposed model can be used to study the aeroelastic performance of long-span bridges under very high wind speed, when nonlinear effects are expected to become significant. The nonlinear buffeting analysis at high wind speed (70 m/s) shows that the geometric and aerodynamic nonlinearities have significant influence on the vertical and torsional displacements while having a small effect on the lateral displacement.

Acknowledgments

This work was supported by the National Science Foundation of China (Project No. 51278064; 51108154 and 51408053), the Fundamental Research Funds for the Central Universities (2013G2211002), 973 project of P.R. China, under the contract of 2015CB057701. The support is greatly appreciated.

References

Bucher, C.G., and Lin, Y.K. (1987), “Stochastic stability of bridges considering coupled modes”, *J. Eng. Mech. - ASCE*, **12**, 2055-2071.

Baker, C.J. (1994), “The quantification of accident risk for road vehicles in cross winds”, *J. Wind Eng. Ind. Aerod.*, **52**, 93-107.

Cai, C.S. and Chen, S.R. (2004), “Framework of vehicle-bridge-wind dynamic analysis”, *J. Wind Eng. Ind. Aerod.*, **92**(7-8), 579-607.

Chen, S.R. and Cai, C.S. (2004), “Accident assessment of vehicles on long-span bridges in windy environments”, *J. Wind Eng. Ind. Aerod.*, **92**(12), 991-1024.

Chen, S.R. and Cai, C.S. (2007), “Equivalent wheel load approach for slender cable-stayed bridge fatigue assessment under traffic and wind: Feasibility study”, *J. Bridge Eng. - ASCE*, **12**(6), 755-764.

Chen, S.R. and Wu, J. (2010), “Dynamic performance simulation of long-span bridge under combined loads of stochastic traffic and wind”, *J. Bridge Eng. - ASCE*, **13**(3), 219-230.

Chen, S.R. and Wu, J. (2011), “Modeling stochastic live load for long-span bridge based on microscopic traffic flow simulation”, *Comput. Struct.*, **89**(9-10), 813-824.

Cao, Y.H., Xiang, H.F. and Zhou, Y. (2000), “Simulation of stochastic wind velocity field on long-span bridges”, *J. Eng. Mech. - ASCE*, **126**(1), 1-6.

Chen, Z.W., Xu, Y., L., Li, Q. and Wu, D.J. (2011), “Dynamic stress analysis of long suspension bridges under wind, railway, and highway loadings”, *J. Bridge Eng. - ASCE*, **16**(3), 383-391.

Chen, A.R. and Ma, R.J. (2004), *Report on the wind tunnel experiments of Su tong cable-stayed bridge, Dept. of Bridge Engineering, Tongji Univ.*, Shanghai, China.

Chen, A.R., You, Q.Z., Zhang, X.G., Ma, R.J. and Zhou, Z.Y. (2005), “Aerodynamic problems of a long span cable-stayed bridge”, *Proceedings of the IABSE Symp., International Association for Bridge and Structural Engineering,* Zurich, Switzerland.

Cheung, M.S. and Chan, Y.B. (2010), “Operational requirements for long span bridges under strong wind events”, *J. Bridge Eng.- ASCE,* **15**(2), 131-143.

Davenport, A.G. (1968), “The dependence of wind load upon meteorological parameters”, *Proceedings of the International Research Seminar on Wind Effects on Building and Structures*, University of Toronto Press, Toronto.

Ding, Q. and Lee, P.K.K. (2000), “Computer simulation of buffeting actions of suspension bridges under turbulent wind”, *Comput. Struct.*, **76**,787-797.

Ernst, J.H. (1965), “Der e-modul von seilen unter berucksichtigung desdurchhanges”, *Der Bauingenieur*, **40**(2), 52-55 (in German).

Han, W.S., Ma, L., Yuan, S.J. and Wang, B. (2011), “Three-dimensional coupling vibration of wind-vehicle-bridge systems under random traffic flow”, *Proceedings of the 13th International Conference on Wind Engineering,* Amsterdam, the Netherlands.

Han, W.S., Yuan, S.J. and Ma, L. (2014a), “Vibration of vehicle-bridge coupling system with measured correlated road surface roughness”, *Struct. Eng. Mech.*, **51**(2), 315-331.

Han, W.S., Wu, J., Cai, C.S. and Chen, S.R. (2014b), “Characteristics and dynamic impact of overloaded extra heavy trucks on typical highway bridges”, *J. Bridge Eng. – ASCE* (in press).

International Organization for Standardization (ISO) (1995), *Mechanical vibration-road surface profiles-reporting of measured data*, ISO 8068:(E), ISO, Geneva.

Kaimal, J.C., Wyngaard, J.C., Izumi, I. and Cote, O.R. (1972), “Spectral characteristics of surface-layer tursbulence”, *Q. J. R. Meteorol. Soc.*, **98**(417), 563-589.

Li, Y.L., Qiang, S.Z., Liao, H.L. and Xu, Y.L. (2005), “Dynamics of wind-rail vehicle-bridge systems”, *J. Wind Eng. Ind. Aerod.*, **93**(6), 483-507.

Li, Y.L., Xiang, H.Y., Wang, B., Xu, Y.L. and Qiang, S.Z. (2013), “Dynamic analysis of wind-vehicle-bridge system with two trains interaction”, *Adv. Struct. Eng.*, **16**(10), 1663-1670.

Li, Q., Xu, Y.L., Wu, D.J. and Chen, Z.W. (2010), “Computer-aided nonlinear vehicle-bridge interaction analysis", *J. Vib. Control*, **16**(12), 1791-1816.

Lumley, J.L. and Panofsky, H.A. (1964), *The Structure of Atmospheric Turbulence*, Wiley, New York.

Ma, L., Han, W.S., Ji, B.H. and Liu, J.X. (2014), "A study on the probability of overturning for vehicles moving on a bridge deck in a wind environment considering stochastic process characteristics of excitations", *J. Perform. Constr. Fac.* (in press).

Ministry of Transport of the People's Republic of China (MTPRC) (2004), *Wind-resistant Design Specification for Highway Bridges*, Department of Transportation, China.

Pan, J.Y. and Cheng, Q.G. (1994), "Finite displacement analysis of large suspension bridge", *Civil. Eng.*, **27**(1), 1-9.

Scanlan, R.H. (1978), "The action of flexible bridge under wind, Part II: Buffeting theory", *J. Sound Vib.*, **60**(2), 201-211.

Simiu, E. and Scanlan, R.H. (1996), *Wind Effects on Structures-Fundamentals and Applications to Design*, 3rd Ed., Wiley, New York.

Shinozuka, M. and Deodatis, G. (1991), "Simulation of stochastic processes by spectral representation", *Appl. Mech. Rev.*, **44**(4), 191-204.

Xu, Y.L. and Guo, W.H. (2003), "Dynamic analysis of coupled highway vehicle and cable-stayed bridge systems under turbulent wind", *Eng. Struct*., **25**(4), 473-486.

Xu, Y.L., Li, Q., Wu, D.J. and Chen, Z.W. (2010), "Stress and acceleration response analysis of vehicle-bridge systems using mode superposition method", *Eng. Struct*., **32**(5), 1356-1368.

Xia, H., Guo, W.W., Zhang, N. and Sun G.J. (2008), "Dynamic analysis of a train–bridge system under wind action", *J. Eng. Mech. - ASCE*, **86**(19-20), 1845-1855.

Yang, F. and Fonder, G. (1996), "An iterative solution method for dynamic response of bridge-vehicles systems", *Earthq. Eng. Struct. D*., **25** (2), 195-215.

Zhang, X.J., Xiang, H.F. and Sun, B.N. (2002), "Nonlinear aerostatic and aerodynamic analysis of long-span suspension bridges considering wind-structure interactions", *J. Wind Eng. Ind. Aerod*., **90**(2), 1065-1080.